Physical Modeling of Surface and Heterojunction for Mesa-Structured HBTs

Edwin C. Kan and Robert W. Dutton
Applied Electronics Lab 201, Stanford University, Stanford, CA 94305

Abstract – Mesa-structured heterojunction bipolar transistors are analyzed by 2D device simulation, with emphasis on the treatment of exposed base surface and emitter-base heterojunction. Physical models for surface (surface recombination velocity and surface traps) and heterojunction (thermionic/diffusion and base dopant back diffusion) are compared to illustrate their effects on terminal characteristics. A strategy to assure accurate modeling is suggested.

I. Introduction

Accurate device modeling of HBTs is critical for the optimal design in analog circuit applications. Often arbitrary contact resistances and recombination lifetimes are employed to fit the experimental curves. However, this practice not only obscures the physical relevance of each effect, but also makes design scaling and parasitic network extraction very difficult. A *truly* calibrated device model should include all physical effects that can significantly affect the dc and ac terminal characteristics. In this paper, the choice of physical models for partially passivated surfaces, heterojunction transport, and the consideration of base-dopant back diffusion will be examined. Suggestions on modeling strategy and design trade-offs with respect to these effects will be summarized.

II. Modeling of Partially Passivated Surface

For mesa structure HBTs, the imperfect exposed surface has a strong influence on the dc and ac behavior. Traditionally, either mid-gap surface traps or surface recombination is used to model the surface fermi level pinning. The surface-trap approach will pin both the majority and minority fermi levels, while the surface-recombination approach will only affect the minority carrier. Also, the electric potential distribution in the insulator above the exposed surface will be different. The difference is reflected in the terminal characteristics. This is because the influence of surface traps will come from the charged-trap term in the Poisson equation with the charged percentage governed by the dynamic trap equation:

$$\nabla(\epsilon\nabla\psi) = q(n - p - N_D^+ + N_A^- - N_{DD}^+ + N_{AA}^-) \qquad (1)$$

$$\frac{\partial N_{DD}^+}{\partial t} = (C_{pn}p + e_{nn})(N_{DD} - N_{DD}^+) - (C_{nn}n + e_{pn})N_{DD}^+ \qquad (2)$$

$$\frac{\partial N_{AA}^-}{\partial t} = (C_{np}n + e_{pp})(N_{AA} - N_{AA}^-) - (C_{pp}p + e_{np})N_{AA}^- \qquad (3)$$

where ψ is the potential, ϵ the dielectric constant, q the elementary charge, n and p the electron and hole concentrations, N_D^+ and N_A^- the ionized dopants, N_{DD}^+ and N_{AA}^- the charged traps (only one charge state is considered), and C and e for trap capture and emission rates. The surface recombination velocity modifies the SRH recombination rate $1/\tau_{SRH}$ in the current continuity equation.

$$\frac{1}{\tau_{SRH}^{eff}} = \frac{sd}{A} + \frac{1}{\tau_{SRH}} \qquad (4)$$

where s is the surface recombination velocity, d and A are the length and area of the associated surface element. In Figs. 1 and 2, the HBT [1] used in the simulation[2] is shown. Fig. 3 shows the Gummel plots for a perfectly passivated surface, a surface with very high surface recombination velocity ($10^7 cm/s$) and one with very high surface trap levels ($3 \times 10^{13} cm^{-2}$). It can be observed that these two models for unpassivated surface will give different IV curves. Figs. 4 and 5 show the results of varying the surface trap concentrations and the surface recombination velocity. Figs. 6 and 7 show the carrier concentrations $0.2\mu m$ away from the mesa edge. For surface trap concentration below $10^{12} cm^{-3}$ (or s below $10^2 cm/s$), the surface effects are relatively small both in IV curves and concentration profiles. It is proposed [1] that the passivation of exposed surface is only necessary close to the mesa edge. There are two popular ways to achieve this passivation. First, the emitter layer next to the heterojunction can be extended out for 0.1 to 0.5 μm (MBE process). Second, the exposed surface can be passivated using either photo- or plasma-assisted CVD process. Comparison of simulation results is shown in Figs. 8 and 9.

III. Modeling of Heterojunction Transport

The chirp grading of E-B heterojunctions [1] can be modeled as a series of stair-like barriers using thermionic emssion or by diffusion assuming that tunneling has smeared the barriers. These two approaches are not asymptotically equivalent, since thermionic emission assumes no significant scattering at the interface and treats the left-hand-side and right-hand-side distributions as independent. The interface model *only* considers energy with the tunneling effect as a correction term to the barrier height. Fig. 10 shows the Gummel plots with 8 layers to approximate the heterojunction with parabolic grading. Experimental results are also shown with best fitting to the collector current. It is expected that the base current lies in between the two approaches [3].

IV. Modeling of Base-Dopant Back Diffusion

The back diffusion of base dopants into the emitter region, either during the emitter growth or electrical stress, is known to cause degradation in device performance [4].

						y = 0.000
200Å	n	GaAs	2×10^{18}		Contact	y = 0.020
300Å	n	GaAs	5×10^{17}		Cap	y = 0.050
300Å	n	AlGaAs	5×10^{17}	x = .0 -- .3	CapEmitter Grading	y = 0.080
200Å	n	AlGaAs	5×10^{17}	x = .3	Emitter	y = 0.100
340Å	n	AlGaAs	5×10^{17}	x = .3 -- .0	EmitterBase Grading	y = 0.134
1000Å	p	GaAs	5×10^{18}		Base	y = 0.234
3000Å	n	GaAs	5×10^{16}		Collector	y = 0.534
1000Å	n	GaAs	2×10^{18}		SubCollector	y = 0.634
	n+	GaAs			Substrate	

Figure 1: material and doping used in simulation for mesa-structure HBT.

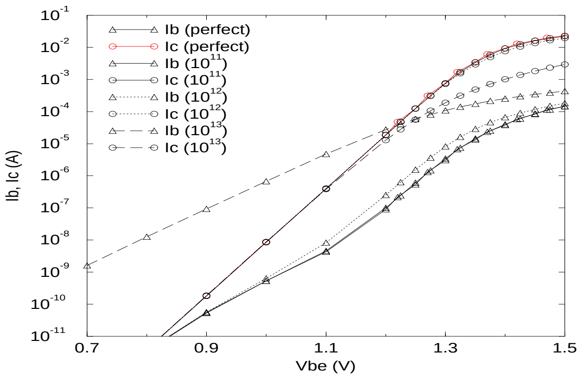

Figure 4: Gummel plots for variation in surface trap levels between 10^{11} and 10^{13} (cm^{-3}).

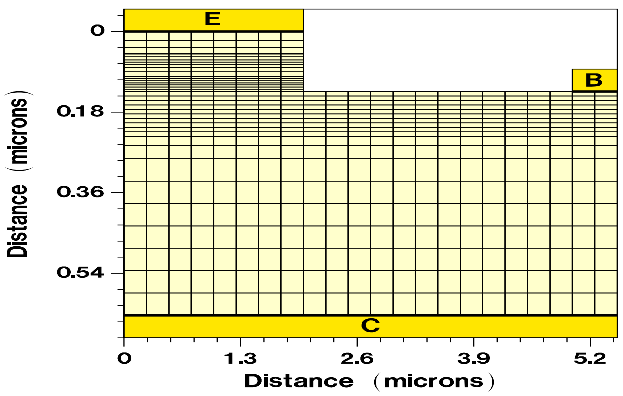

Figure 2: 2-D simulation domain. The gridding will adapt to specific needs below.

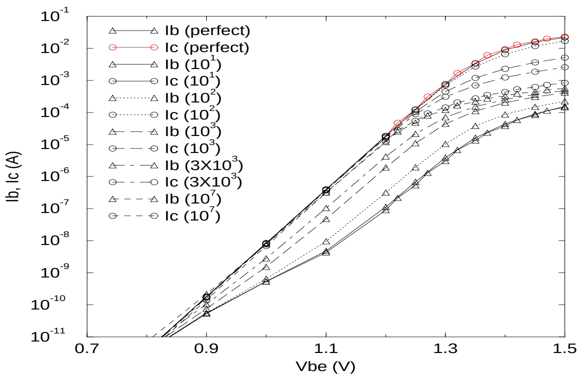

Figure 5: Gummel plots for variation in surface recombination velocity between 10^1 and 10^7 (cm/s).

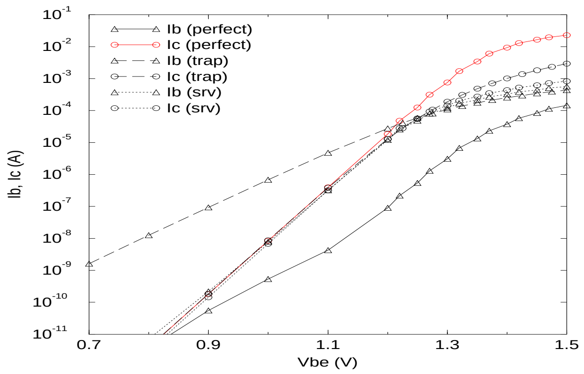

Figure 3: Gummel plots for perfect and damaged surfaces. Both surface damage models are shown (surface recombination velocity and surface traps).

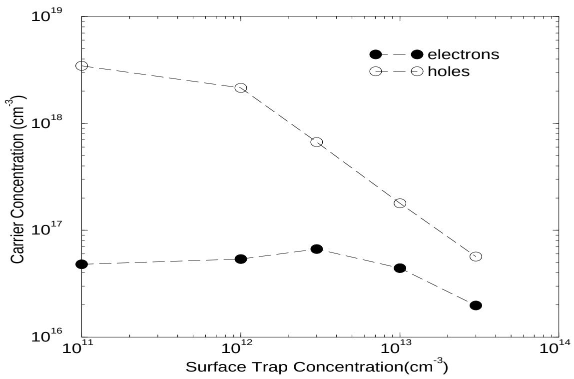

Figure 6: Carrier concentrations at 0.2 μm from emitter edge for various surface trap levels.

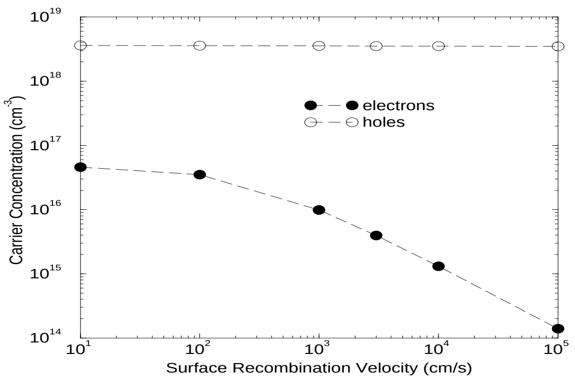

Figure 7: Carrier concentrations at 0.2 μm from emitter edge for various surface recombination velocities.

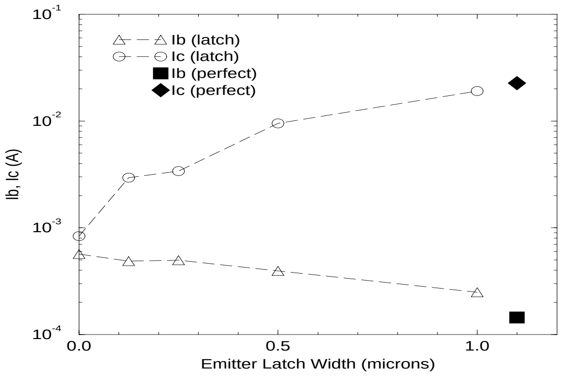

Figure 8: Comparison on various emitter latch width.

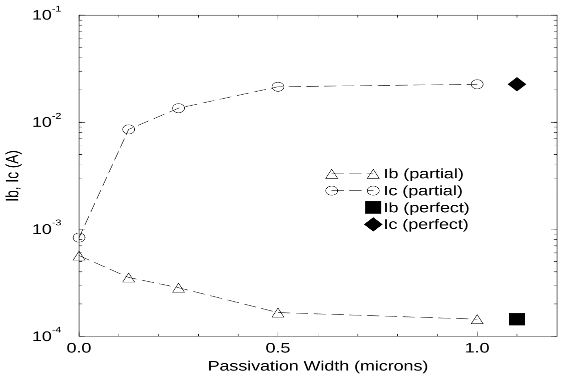

Figure 9: Comparison on various partial surface passivation width.

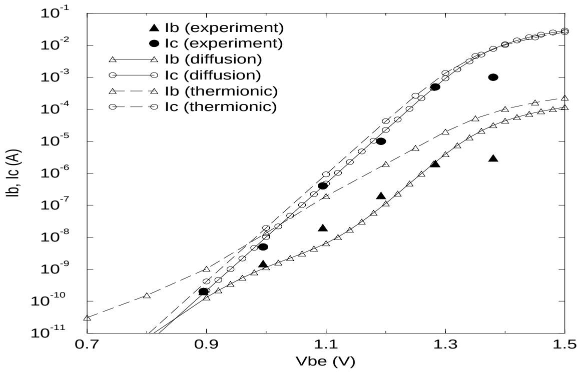

Figure 10: Gummel plots for thermionic emission, diffusion and experiment fit.

The resulting displacement of the material and pn junctions is modeled in [5]. It will be shown below that the degradation is small before the formation of a potential spike [6]. In Fig. 11, the back diffusion is characterized by Gaussian profiles with different standard deviations m_1. The equilibrium band diagrams, the Gummel plots and the frequency responses of h_{21} are presented in Figs. 12-15. Both collector and base currents are reduced with larger back diffusion, while the ideality factor of base current gradually increases. The decrease in f_T is also much more pronounced after the spike is formed. However, this backdiffusion degradation can be much relieved by introducing donor stoppers in the heterojunction. In Fig. 12, stopper 1 is an additional Gaussian profile starts at 0.11 μm and has 10 nm standard deviation. Stopper 2 has 20 nm standard deviation. In Fig. 14, we can see that both collector and base currents are rather insensitive to Be backdiffusion with stoppers (the spacer is not as effective). The conduction band spike is not observed with stopper 2 (Fig. 16). The width of the stopper needs to be optimized though, since additional donor dopants in the emitter will increase the base current, and hence degrade the gain.

Acknowledgements

This work is supported by ARPA Contract No. DABT63-94-C-OOJJ. The authors are thankful to Drs. C. Dai and W. Liu.

References

[1] C. Dai, *Ph.D. Thesis*, Stanford Univ., 1995.
[2] SemiCad Device, v1.3, Dawn Technologies, 1993.
[3] K. Horio, et. al., *IEEE TED*, **37**, 1093(1990).
[4] P. M. Asbeck, et. al., *IEEE TED*, **36**, 2032(1989).
[5] Q. M. Zhang, et. al., *IEEE TED*, **39**, 2430(1992).
[6] H. H. Lin, et. al., *IEEE EDL*, **EDL-6**, 431(1985).

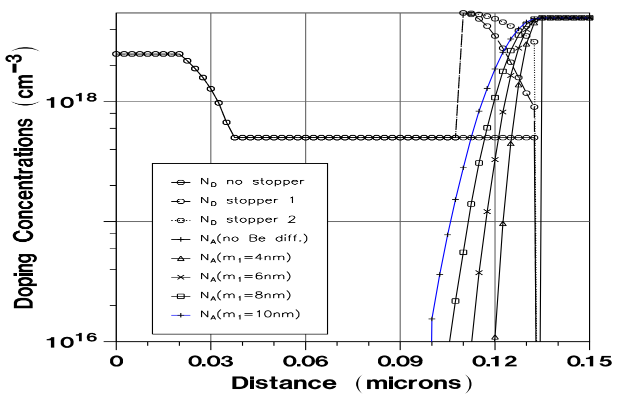

Figure 11: Back diffusion doping profiles. Possible donor stoppers are also shown.

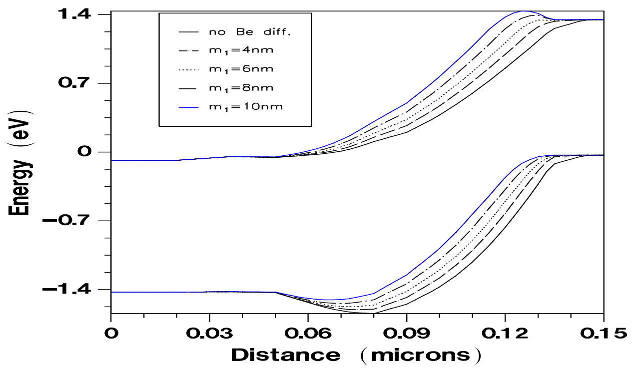

Figure 12: Bands for various back diffusion profiles without stopper.

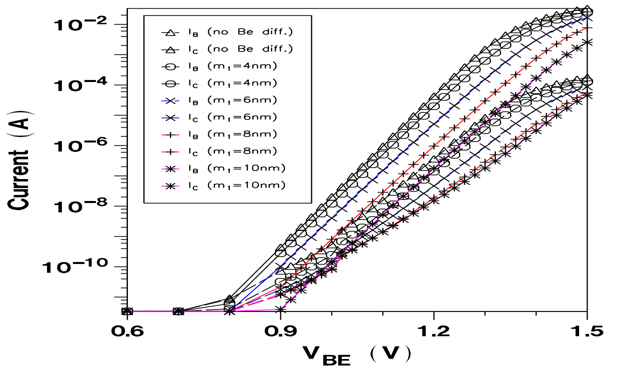

Figure 13: Gummel plots with varying m_1 without stopper.

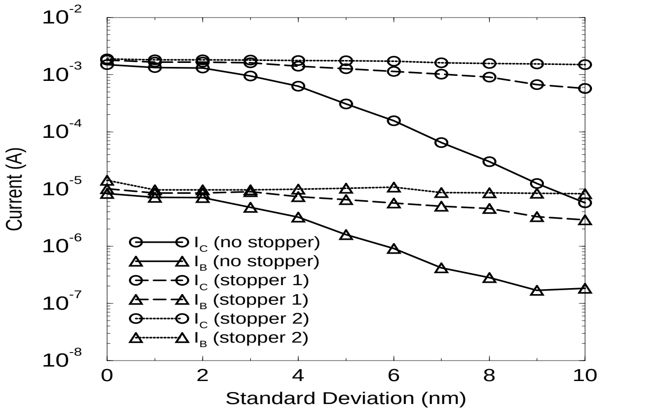

Figure 14: Terminal currents with varying m_1 with and without stopper.

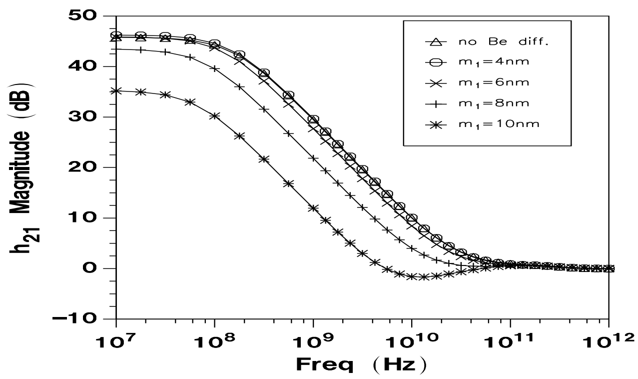

Figure 15: h_{21} for various back diffusion profiles without stopper.

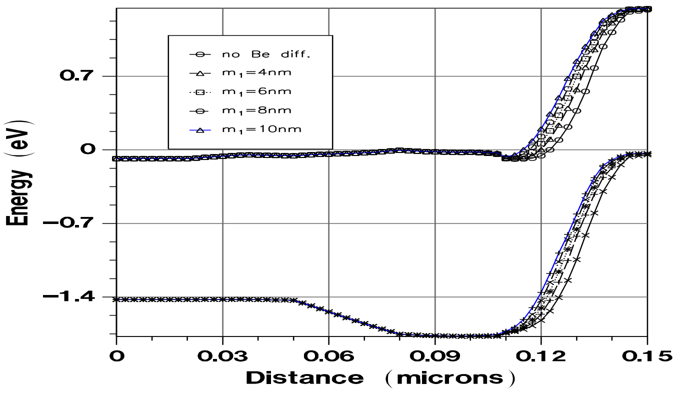

Figure 16: Bands for various back diffusion profiles with donor stopper 2.